

Article

# Enhanced Reversible Magnetic-Field-Induced Strain in Ni-Mn-Ga Alloy

Pingping Wu<sup>1,2,\*</sup> and Yongfeng Liang<sup>3</sup> <sup>1</sup> Department of Materials Science and Engineering, Xiamen Institute of Technology, Xiamen 361021, China<sup>2</sup> The Higher Educational Key Laboratory for Flexible Manufacturing Equipment Integration of Fujian Province, Xiamen Institute of Technology, Xiamen 361021, China<sup>3</sup> State Key Laboratory for Advanced Metals and Materials, University of Science and Technology Beijing, Beijing 100083, China; liangyf@skl.ustb.edu.cn

\* Correspondence: pingpingwu@xit.edu.cn

**Abstract:** A phase-field model was developed to simulate the ferromagnetic domain structure and martensite variant microstructure of Ni-Mn-Ga shape-memory alloy. The evolution of reversible magnetic-field-induced strain (MFIS) and associated magnetic domain/martensite variant structure were modeled under an external magnetic field. It was found that MFIS increased significantly from 0.2% to 0.28% as the temperature increased from 265 K to 285 K. In addition, compressive pre-stress efficiently enhanced the MFIS of the alloy, while tensile stress reduced MFIS. Furthermore, it was proved that there was possibility of achieving similar enhancement of MFIS by replacing compressive stress with perpendicular biaxial tensile stress. The results revealed that the residual variant induced by stress plays an important role in the reversible MFIS effect.

**Keywords:** phase-field model; magnetic-field-induced strain; Ni-Mn-Ga alloys; ferromagnetic shape-memory alloy



**Citation:** Wu, P.; Liang, Y. Enhanced Reversible Magnetic-Field-Induced Strain in Ni-Mn-Ga Alloy. *Metals* **2021**, *11*, 2017. <https://doi.org/10.3390/met11122017>

Academic Editor: Alberto Moreira Jorge, Jr.

Received: 17 October 2021  
Accepted: 6 December 2021  
Published: 13 December 2021

**Publisher's Note:** MDPI stays neutral with regard to jurisdictional claims in published maps and institutional affiliations.



**Copyright:** © 2021 by the authors. Licensee MDPI, Basel, Switzerland. This article is an open access article distributed under the terms and conditions of the Creative Commons Attribution (CC BY) license (<https://creativecommons.org/licenses/by/4.0/>).

## 1. Introduction

The  $L2_1$  structure of Heusler compound  $Ni_2MnGa$  has attracted much attention in the last few decades. Since the large magnetic-field-induced strain (MFIS) was discovered, this intermetallic material has been a potential candidate for a wide variety of possible applications, such as actuators, sensors, etc. [1–4]. Today, there are two major concerns for this alloy system for researchers. One is pursuing larger MFIS [5–7], as seen in 5 M [8], 7 M and NM [9] structures. The other concern is the stress–strain property of Ni-Mn-Ga alloy, as the traditional shape-memory alloy exhibits martensite transformation. Specifically, high strain can be caused by thermoelastic martensite transformations (so-called superelasticity [10,11]), or driven by the conjunction effect by the magnetic field and stress field. Large MFIS comes from the coupling between ferromagnetic domain walls and twin boundaries of martensite variants. The descriptions of magnetic domain structures and martensite structures are found in the experimental literature [7,12] and reconstructed in simulation works [13].

For any application of Ni-Mn-Ga alloy, two main difficulties should be addressed. One difficulty is that large MFIS requires a single-crystal alloy. In terms of a polycrystalline material, if the grain direction is almost random, the physical behavior of the multi-grained alloy is an average of the behavior of single crystals of all orientations. Therefore, in order to achieve the properties similar to a single-crystal material, the grain texture should be processed to make more grain orientations towards the same direction. Dunand et al. [14–16] improved the MFIS of multi-grained Ni-Mn-Ga alloy by controlling the grain size and shape. Zhou et al. [17] employed a directional solidification process to control the multi-grained texture. The other issue is that the irrecoverable MFIS of Ni-Mn-Ga alloy makes it difficult in applications. To address this problem, Hua et al. [18] developed

a metamagnetic single-crystalline NiCuCoMnGa alloy to receive reversible strain and practice many thermo-mechanical training cycles to improve MFIS. Yu et al. [19] increased the value of MFIS to 0.49% by doping In ions in polycrystalline Ni-Mn-Ga alloy. Zhou et al. [17] reported the reversible MFIS in a directionally solidified alloy was up to 0.2%. They found the internal stress supported the enhancement of the reversible strain through superelastic training.

The phase-field model has been extensively used in computer simulations of the structures [13,20,21], stress-strain curves [22] and magnetic field-strain relationships [23,24] of ferromagnetic shape-memory alloys. The model can predict mesoscale microstructures and their evolution under the action of an applied field without a priori assumptions and tracing boundaries. The defects induced by stress are also thought to play an important role in martensite transformation [25,26]. The main purpose of this paper is to perform a phase-field model to describe the domain/martensite microstructures and MFIS response in the presence of residual variant, induced by the defect strain field, and to propose a mesoscale mechanism to explain the reversible MFIS of Ni-Mn-Ga alloy. The MFIS of samples with different temperatures and different magnitudes of applied pre-stress are also studied.

## 2. Phase-Field Model

The components of magnetization ( $M_i$ ) and stress-free strain ( $\varepsilon_{ij}^0$ ) were chosen as the order parameters in the phase-field model, to describe the ferromagnetic domain structure and martensite variants microstructure, respectively. There were three main contributions to the total free energy of Ni<sub>2</sub>MnGa alloy: energy contributions of a ferromagnetic body, energy contributions of martensite variants and the energy contribution of the magneto-elastic effects, i.e.,

$$F_{total} = F_{magnetic} + F_{martensite} + F_{magnetoelastic} \quad (1)$$

where

$$F_{magnetic} = \int \left\{ \begin{array}{l} K_{u1}(m_1^2 m_2^2 + m_2^2 m_3^2 + m_3^2 m_1^2) + K_{u2}(m_1^2 m_2^2 m_3^2) \\ + A(\nabla \vec{m})^2 - \frac{1}{2} \mu_0 M_s (\vec{H}_d \cdot \vec{m}) - \mu_0 M_s (\vec{H}_e \cdot \vec{m}) \end{array} \right\} dV, \quad (2)$$

$$F_{martensite} = \int \left\{ \begin{array}{l} Q_1 e_1^2 + Q_2(e_2^2 + e_3^2) + Q_3 e_3(e_3^2 - 3e_2^2) \\ + Q_4(e_2^2 + e_3^2)^2 + Q_5(e_4^2 + e_5^2 + e_6^2) \\ + \frac{1}{2} g \sum_{i=1}^3 \left[ \left( \frac{\partial \varepsilon_{ii}^0}{\partial x} \right)^2 + \left( \frac{\partial \varepsilon_{ii}^0}{\partial y} \right)^2 + \left( \frac{\partial \varepsilon_{ii}^0}{\partial z} \right)^2 \right] \\ + \frac{1}{2} \sum_{ij,k,l=1}^3 [C_{ijkl}(\varepsilon_{ij} - \varepsilon_{ij}^0)(\varepsilon_{kl} - \varepsilon_{kl}^0)] \end{array} \right\} dV, \quad (3)$$

$$F_{magnetoelastic} = \int \left\{ B \left[ \varepsilon_{11}^0 \left( m_1^2 - \frac{1}{3} \right) + \varepsilon_{22}^0 \left( m_2^2 - \frac{1}{3} \right) + \varepsilon_{33}^0 \left( m_3^2 - \frac{1}{3} \right) \right] \right\} dV, \quad (4)$$

where  $m_i = M_i/M_s$  are the components of the unit magnetization vector,  $M_s$  is the saturation magnetization,  $K_{u1}$  and  $K_{u2}$  are magnetic anisotropy constants,  $A$  is the exchange coefficient,  $\mu_0$  is vacuum permeability,  $H_d = NM$  is the demagnetization field, where  $N$  is the demagnetization factor related to the shape of the material,  $H_e$  is the external applied magnetic field,  $Q_1 \sim Q_5$  are bulk chemical free energy coefficients,  $e_i$  is the symmetry-adapted strain defined in terms of the transformation strains,  $g$  is the strain gradient coefficient,  $C_{ijkl}$  is the elastic stiffness tensor and  $B$  is the magnetoelastic coupling coefficient.

With all the energy contributions, the evolution of non-equilibrium initial random magnetization in Ni-Mn-Ga can be described by the Landau–Lifshitz–Gilbert (LLG) equation:

$$(1 + \alpha^2) \frac{\partial \vec{M}}{\partial t} = -\gamma_0 \vec{M} \times \vec{H}_{\text{eff}} - \gamma_0 \frac{\alpha}{M_s} \vec{M} \times (\vec{M} \times \vec{H}_{\text{eff}}), \quad (5)$$

where  $\alpha$  is the damping constant and  $H_{\text{eff}}$  is the effective magnetic field.

$$\vec{H}_{\text{eff}} = -\frac{1}{\mu_0} \frac{\partial F_{\text{total}}}{\partial \vec{M}}. \quad (6)$$

The LLG equation is solved by employing the Gauss–Seidel projection method in this work [27].

The temporal and spatial evolution of stress-free strain can be described by the Time-Dependent Ginzburg–Landau (TDGL) equation:

$$\frac{\partial \varepsilon_{ii}^0(x, t)}{\partial t} = -L \frac{\delta F_{\text{total}}}{\delta \varepsilon_{ii}^0}, \quad (7)$$

where  $L$  is the kinetic coefficient and the TDGL equation is solved by the semi-implicit Fourier spectral method [28].

It should be noted, according to Khachatryan’s theory [29], that two types of elastic boundary conditions were adopted in this work. One was the constrained boundary condition, under which it was assumed that the homogeneous strain of the system was zero or a fixed value, and the initial ferromagnetic domain structure and martensite microstructure were generated. The other was the stress-free condition, under which it was assumed that the homogeneous strain was an average value of local strain in the system. With this boundary condition, the total strain induced by an external magnetic field or stress field could possibly be calculated. The details of the calculations of elastic energy can be found in previous works [23,27].

### 3. Results

The coefficients for Ni<sub>2</sub>MnGa alloy used in the numerical simulation were as follows [13,30–33]:  $M_s = 6.02 \times 10^5$  A/m,  $K_{u1} = 2.7 \times 10^3$  J/m<sup>3</sup>,  $K_{u2} = -6.1 \times 10^3$  J/m<sup>3</sup>,  $A = 2 \times 10^{-11}$  J/m. The demagnetization factor  $N_x = N_y = N_z = 1/3$  was set for a 3D simulation. The Landau free energy coefficients were obtained based on experimental measurements [30,32]:  $Q_1 = 2.32 \times 10^{11}$  J/m<sup>3</sup>,  $Q_{20} = 3.78 \times 10^8$  J/m<sup>3</sup>,  $Q_2 = Q_{20} (T - T_M)/T_M$ , where  $T$  is the environmental temperature in Kelvin and  $T_M = 300$  K is the martensite transformation temperature for Ni<sub>2</sub>MnGa alloy,  $Q_3 = 0.40 \times 10^{10}$  J/m<sup>3</sup>,  $Q_4 = 7.50 \times 10^{10}$  J/m<sup>3</sup> and the strain gradient  $g = 1.0 \times 10^{-8}$ . The bulk cubic elastic constants of Ni<sub>2</sub>MnGa alloy were  $C_{11} = 1.60 \times 10^{11}$  N/m<sup>2</sup>,  $C_{12} = 1.52 \times 10^{11}$  N/m<sup>2</sup> and  $C_{44} = 0.43 \times 10^{11}$  N/m<sup>2</sup> [33]. The magnetoelastic energy coefficient was  $B = 2.00 \times 10^6$  J/m<sup>3</sup>. To save computational time and memory resources, the simulation was performed with  $32\Delta x \times 32\Delta y \times 32\Delta z$  discrete cells, as  $\Delta x$ ,  $\Delta y$  and  $\Delta z$  are grid spacing. Periodic boundary conditions were applied along all three axes, and the energy was minimized without any applied stress. A randomly distributed defect strain field was used in the simulation. The defect concentration was assumed to be 5%.

Figure 1 shows the temporal evolution of the magnetic domain structure and the martensite variant microstructure in the presence of a defect strain field. The temperature was set to  $T = 285$  Kelvin. At first, constrained elastic boundary conditions were employed, that is, the overall size of the system did not change. The initial random distributed magnetization was evolved into small domains, as shown in Figure 1a, and six different magnetic domains were generated due to the magnetic anisotropy energy. As the initial strain was very small, no martensite variants were observed in the martensite microstructure. After 10,000 computational time steps, the layered lamellae form of  $y/z$  domains was observed, separated by a 90-degree domain wall in the magnetic figure (Figure 1b). In the structure of

martensite variants, corresponding B/C variants were generated, but they were randomly distributed. Finally, a stripe-shaped magnetic domain structure was formed to reduce the magnetostatic energy, as shown in Figure 1c. It should be noted that magnetizations between neighboring lamellae layers were separated by a 180-degree domain wall. In the martensite structure, a polytwinned structure of B/C variants was formed. According to the magnetoelastic coupling effects, it is rather easy to understand the sequential appearance of variants B/C since the magnetization along  $y/z$  directions favors the formation of variants B/C over variants A.

To study the MFIS effect in the simulation, the stress-free boundary condition was used, based on previously generated structures. Figure 1d shows a typical twinned tetragonal phase, variant B/C, with the shorter lattice parameter along the  $y/z$  direction under the stress-free boundary conditions. The simulated structure was consistent with the previous experimental results. Interestingly, the magnetization vector was oriented along the easy magnetization axis and was associated with the martensite variants. The 90-degree domain walls straightened and coincided with the twin boundary. Some residuals of variant A were observed in the martensite structure. It should be noted that the estimated value of strain field of variant A caused by defects was set as  $\epsilon_{11} = -0.006$  in the work so as to clearly demonstrate the change in the martensite structure and the motion of the twin boundary.

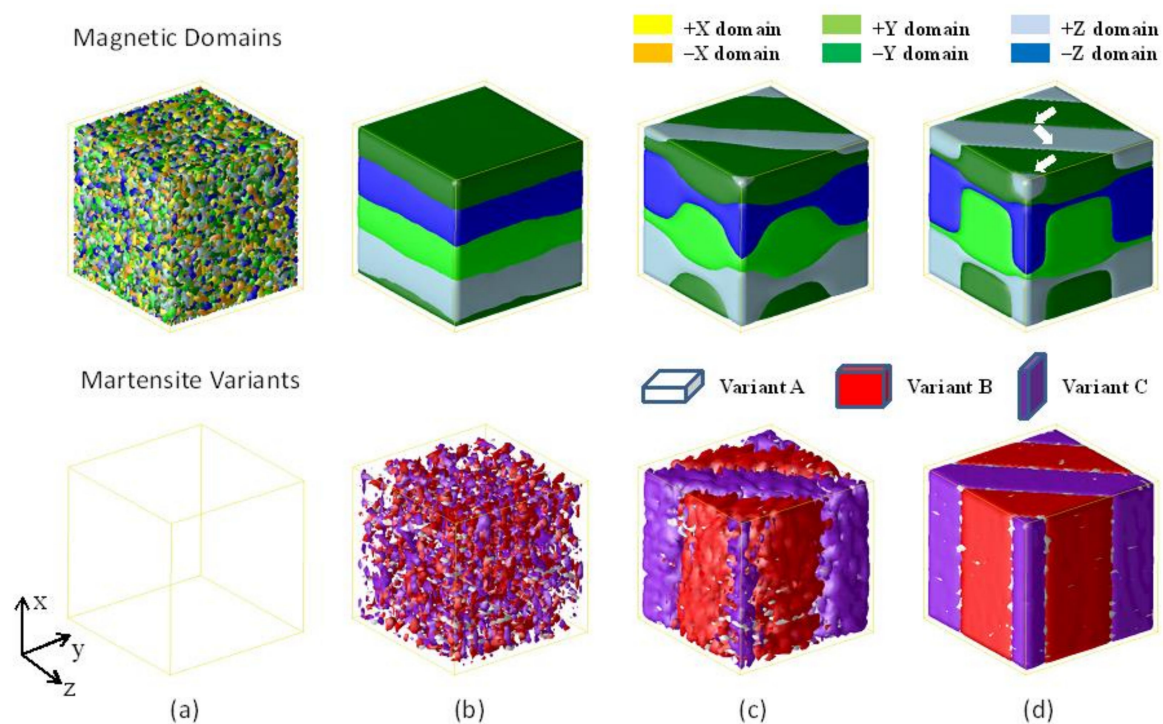


**Figure 1.** Temporal evolution of ferromagnetic domain morphologies and martensite variant structures with clamped boundary conditions at (a) 0 steps; (b) 10,000 steps; (c) 30,000 steps, at 285 K. (d) Final structures with stress-free boundary conditions.

The magnetic M-H loop and the MFIS loop of Ni-Mn-Ga alloy at 285 K are illustrated in Figure 2a,b. MFIS reached the maximum value of 0.28% when the magnetization was fully saturated at a field of 0.6 Tesla. In the process of magnetization, the magnetization rotated towards the direction of the external magnetic field. The twin boundary motion of the residual martensite A with a small strain change was observed in the martensite structure. When the magnetization was fully saturated, the MFIS reached the maximum value in the magnetic field direction. In the demagnetization stage, both the magnetization and MFIS returned to zero with a narrow hysteresis. The magnetization rotated back to its initial status because of the magnetoelastic coupling effect between the martensite variants

and magnetization. Finally, a recoverable magnetic-field-induced strain was obtained in the simulation.

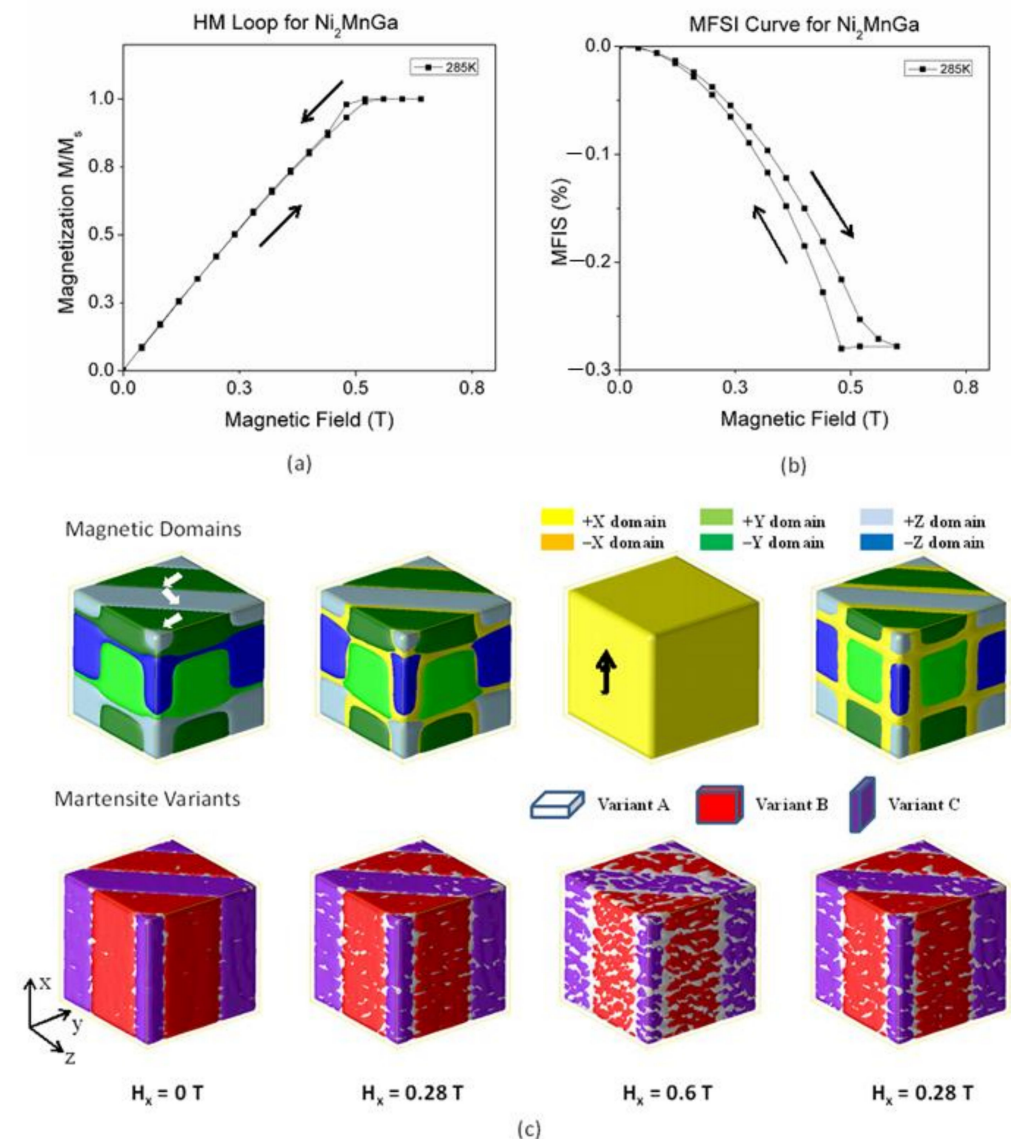


**Figure 2.** The field dependence of magnetization and magnetic field-induced strain (MFIS) for Ni-Mn-Ga alloy. (a)  $M/M_s$  vs. applied field curves; (b) MFIS vs. applied field curves; (c) the ferromagnetic domain structure and martensite variant evolution under applied field along the  $x$ -axis (without stress).

The simulations at different temperatures were carried out in the work to test the sensitivity of reversible strain to temperature. As shown in Figure 3, similar recoverable strain curves were obtained, but MFIS decreased when lowering the temperature. It should be noted that the eigen-strain increased as the environmental temperature decreased, leading to enhanced magnetoelastic coupling between variants and magnetic domains. When an out-of-plane magnetic field ( $H_x$ ) perpendicular was applied to the in-plane field preferred variants, it was difficult to maintain high reversible MFIS in the Ni-Mn-Ga alloy.

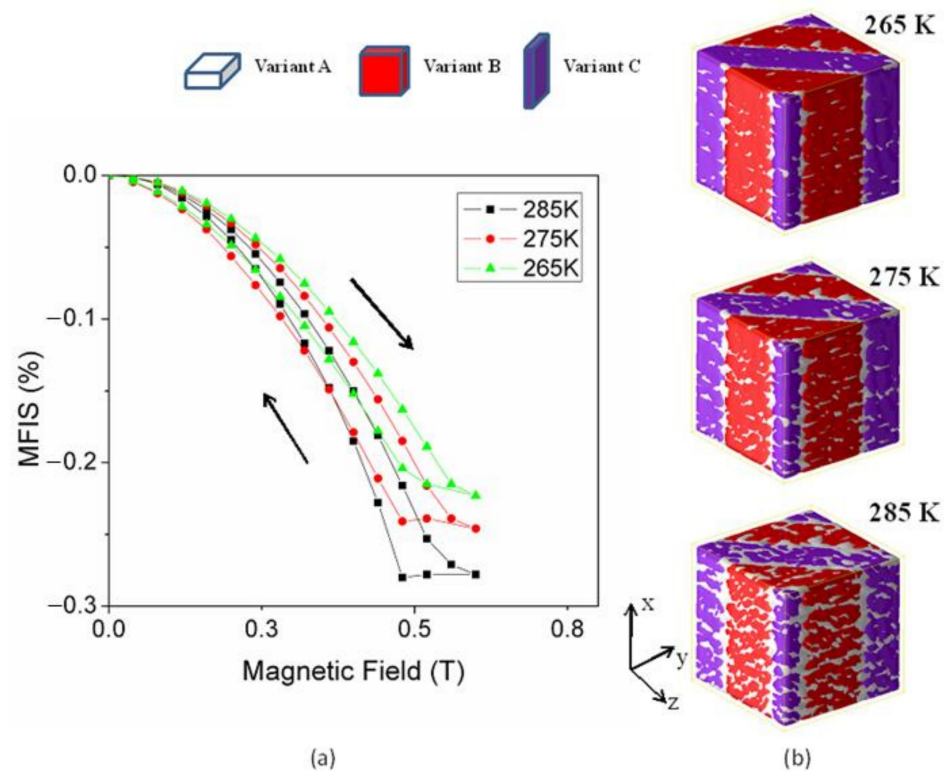


**Figure 3.** (a) The MFIS loops at 285 K, 275 K and 265 K, respectively. (b) The simulated martensite variant structure at  $H_x = 0.6$  T.

The previous simulation results showed that MFIS is strongly influenced by applied stress. It can be easily seen that compressive stress, which produces an elongation in the  $x$ -axis, energetically favors variant A, while tensile stress favors variants B and C. The evolution of MFIS and its related martensite variant structure of the samples with compressive applied stress along the  $x$ -axis under the applied magnetic field is shown in Figure 4. The ambient temperature was assumed to be 285 K. With the increase in applied compressive stress from 0 MPa to 3 MPa, the MFIS of the sample increased from 0.28% to 0.38%. As expected, the compressive stress increased the strain field induced by residual variant A, as shown in Figure 4b. Under the action of an external magnetic field, the growth of variant A was observed, and the overall strain response increased due to the movement of the martensite twin boundary. It should be pointed out that the MFIS returned to zero when the magnetic field was completely removed, but a larger hysteresis loop was observed. This reversible strain can be attributed to the low pre-applied compressive stress, which led to a reversible variant boundary movement. In addition, under higher compressive stress, the magnetization and MFIS cannot return to their original state because of the irreversible variant boundary movement.

The effect of tensile stress on MFIS and martensite variant structure was also studied. Figure 5 shows MFIS vs. magnetic field curves and related variant structures at tensile stress of 1 MPa~3 MPa. MFIS decreased to 0.21% and the strain field surrounding variant A was seen to be reduced under the influence of the tensile stress. MFIS was still reversible and led to small hysteresis.

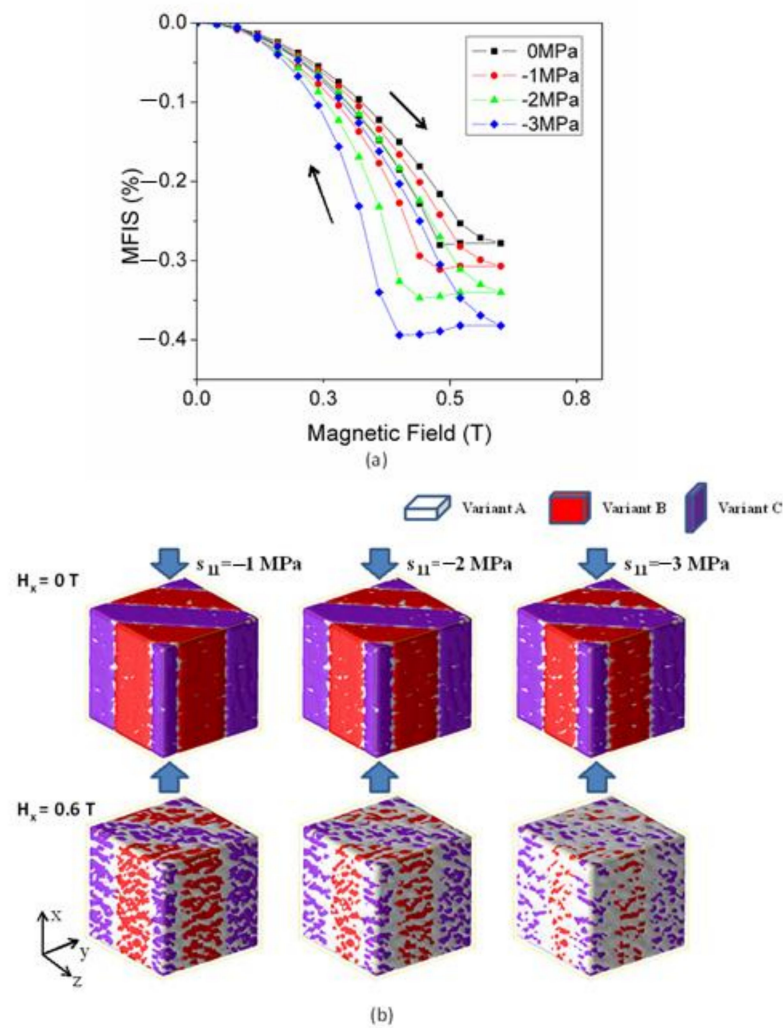


**Figure 4.** (a) MFIS loops with different applied compressive stress (along the  $x$ -axis) at 285 K; (b) simulated martensite variants at  $H_x = 0$  T and  $H_x = 0.6$  T.

In previous experiments, it was found to be difficult to apply the magnetic field and stress field in the same direction. Therefore, the stress field is usually applied in a direction perpendicular to the direction of the magnetic field in current experiments. It is necessary to find a possible alternative method for experiments to check the effect of stress on reversible MFIS behavior. In the simulation, biaxial stress was employed on the directional Ni-Mn-Ga alloy. As shown in the inset of Figure 6, tensile/compressive stress was pre-applied in both the  $y$ - and  $z$ -direction to replace the compressive/tensile stress applied in the  $x$ -direction. As strain-magnetic field loops measured the average strain of the system, the effect of such biaxial stress on the surrounding strain field of variant A was equal to the uniaxial stress along the  $x$ -axis. As shown in Figure 6, a minor difference was observed in MFIS loops.

As mentioned above, we performed a mesoscopic phase-field simulation considering the reversible MFIS at a defect concentration of 5%. It was proposed that the residual variant A was caused by the defects, which resulted in the reversible variant wall movement and reversible MFIS at an external magnetic field. It should be noted that the defect concentration can be controlled by doping impurity atoms. At low defect concentrations ( $c = 0 \sim 0.05$ ), the increase in variant boundaries can enhance the maximum value of MFIS. However, for high defect concentrations, the martensite system may be in a “strain glass” state [25,26], i.e., a frozen disordered strain state, which may lead to a decrease in MFIS. The research work is in progress.

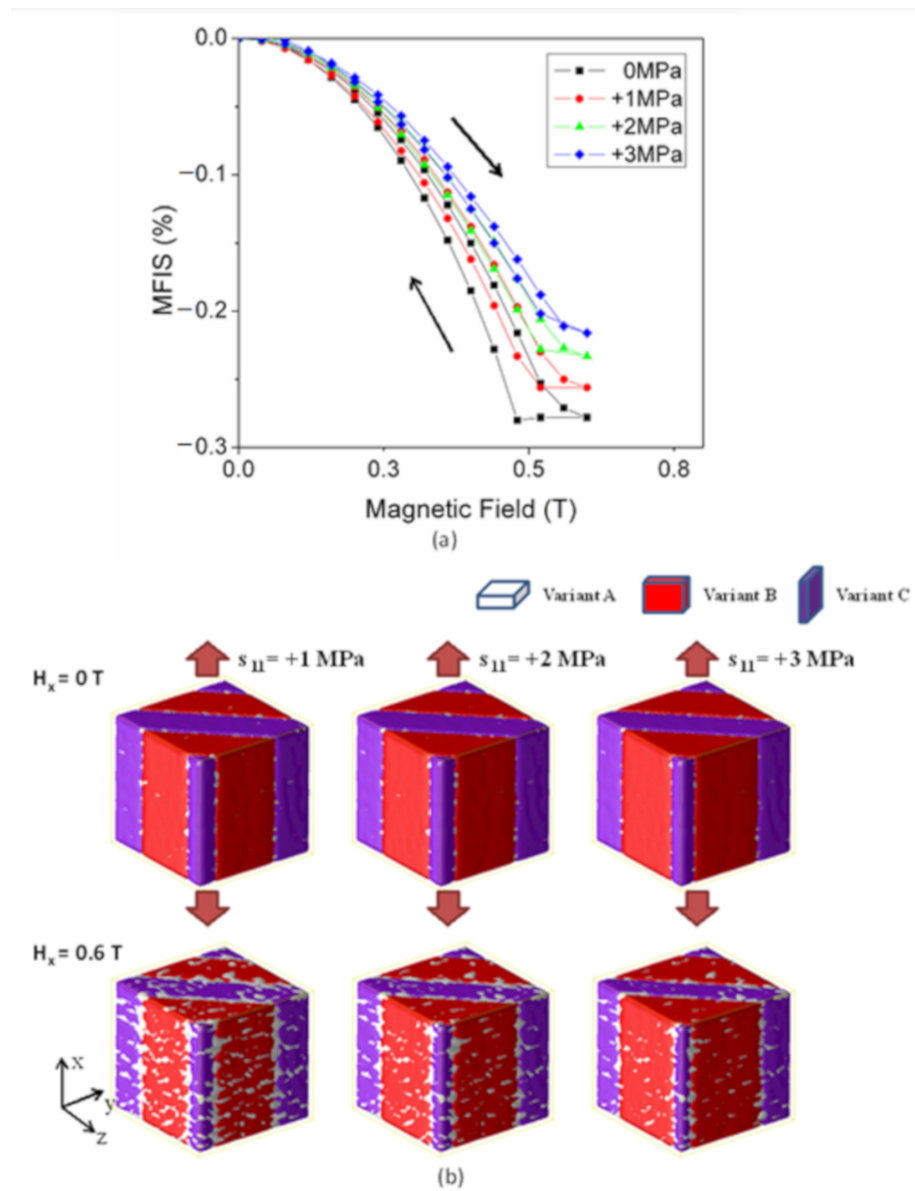


Figure 5. (a) MFIS loops with different applied tensile stress (along the x-axis) at 285 K; (b) simulated martensite variants at  $H_x = 0$  T and  $H_x = 0.6$  T.

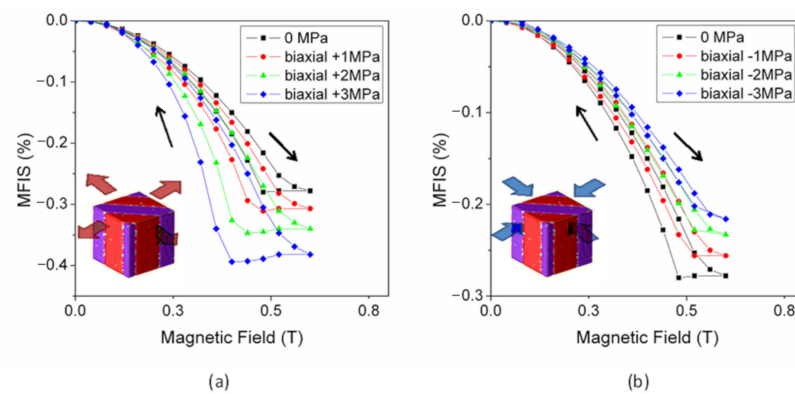


Figure 6. Simulated MFIS loops with different biaxial applied stress at 285 K: (a) biaxial tensile stress along y- and z-axis; (b) biaxial compressive stress along y- and z-axis.

For polycrystalline materials, the grain boundary itself is a general planar defect, which may make a contribution to the total MFIS in experiments. On the other hand, mechanical training may promote the rearrangement of martensite variants with the movement of the twin boundary [17]. This leads to a decrease in the fraction of residual variants. Finally, the phase-field model can simulate the grain textures of elastically inhomogeneous polycrystalline materials and the grain boundary migration under stress [34], and these technologies can be employed to predict and improve the properties of the MFIS of polycrystalline Ni-Mn-Ga alloy in the future.

#### 4. Conclusions

A three-dimensional computational model, combining a micromagnetic method with the phase-field microelastic model, was employed to study the evolution of the ferromagnetic domain and martensite variants in an external applied magnetic field. Reversible MFIS was observed in the simulation, which can be attributed to the residual variant boundary movement led by defects of the samples. The results showed that MFIS increased significantly from 0.2% to 0.28% as the temperature increased from 265 K to 285 K. It was demonstrated that a compressive pre-stress field can be efficiently used to enhance MFIS at a saturation magnetic field. Reversible MFIS was observed, which was due to the reversible variant wall movement under the action of a compressive field. The uniaxial stress field applied along the growth direction can also be replaced by biaxial stress, perpendicular to the growth direction. Therefore, the enhancement of reversible MFIS is potentially relevant to the application of Ni-Mn-Ga alloy in the future.

**Author Contributions:** Conceptualization, P.W. and Y.L.; methodology, P.W.; investigation, P.W.; resources, P.W.; data curation, P.W.; writing—original draft preparation, P.W.; writing—review and editing, Y.L.; visualization, P.W.; project administration, P.W.; funding acquisition, P.W. and Y.L. All authors have read and agreed to the published version of the manuscript.

**Funding:** This work was supported by the State Key Lab for Advanced Metals and Materials in University of Science and Technology Beijing with contract No. 2021-ZD02, the Cultivating Advanced Functional Materials Research Group Program of Xiamen Institute of Technology with contract No. KYTD202004 and the Fundamental Research Funds for the Central Universities (FRF-MP-20-44).

**Institutional Review Board Statement:** Not applicable.

**Informed Consent Statement:** Not applicable.

**Data Availability Statement:** Data sharing is not applicable.

**Conflicts of Interest:** The authors declare no conflict of interest.

#### References

1. O'Handley, R.C.; Murray, S.J.; Marioni, M.; Nembach, N.; Allen, S.M. Phenomenology of giant magnetic-field-induced strain in ferromagnetic shape-memory materials (invited). *J. Appl. Phys.* **2000**, *87*, 4712–4717. [[CrossRef](#)]
2. Ma, J.; Karaman, I.; Noebe, R.D. High temperature shape memory alloys. *Int. Mater. Rev.* **2013**, *55*, 257–315. [[CrossRef](#)]
3. Li, Z.; Hu, W.; Chen, F.; Zhang, M.; Li, Z.; Yang, B.; Zhao, X.; Zuo, L. Large magnetoresistance in a directionally solidified Ni<sub>44.5</sub>Co<sub>5.1</sub>Mn<sub>37.1</sub>In<sub>13.3</sub> magnetic shape memory alloy. *J. Magn. Magn. Mater.* **2018**, *452*, 249–252. [[CrossRef](#)]
4. Cheng, P.; Zhou, Z.; Chen, J.; Li, Z.; Yang, B.; Xu, K.; Li, Z.; Li, J.; Zhang, Z.; Wang, D.; et al. Combining magnetocaloric and elastocaloric effects in a Ni<sub>45</sub>Co<sub>5</sub>Mn<sub>37</sub>In<sub>13</sub> alloy. *J. Mater. Sci. Technol.* **2021**, *94*, 47–52. [[CrossRef](#)]
5. Heczko, O.; Straka, L. Temperature dependence and temperature limits of magnetic shape memory effect. *J. Appl. Phys.* **2003**, *94*, 7139–7143. [[CrossRef](#)]
6. Liang, T.; Jiang, C.B.; Xu, H.B.; Liu, Z.H.; Zhang, M.; Cui, Y.T.; Wu, G.H. Phase transition strain and large magnetic field induced strain in Ni<sub>50.5</sub>Mn<sub>24</sub>Ga<sub>25.5</sub> unidirectionally solidified alloy. *J. Magn. Magn. Mater.* **2004**, *268*, 29–32. [[CrossRef](#)]
7. Karaca, H.; Karaman, I.; Basaran, B.; Chumlyakov, Y.; Maier, H. Magnetic field and stress induced martensite reorientation in NiMnGa ferromagnetic shape memory alloy single crystals. *Acta Mater.* **2006**, *54*, 233–245. [[CrossRef](#)]
8. Pagounis, E.; Chulist, R.; Szczerba, M.J.; Laufenberg, M. Over 7% magnetic field-induced strain in a Ni-Mn-Ga five-layered martensite. *Appl. Phys. Lett.* **2014**, *105*, 052405. [[CrossRef](#)]
9. Sozinov, A.; Lanska, N.; Soroka, A.; Zou, W. 12% magnetic field-induced strain in Ni-Mn-Ga-based non-modulated martensite. *Appl. Phys. Lett.* **2013**, *102*, 021902. [[CrossRef](#)]

10. Chernenko, V.A.; L'vov, V.; Pons, J.; Cesari, E. Superelasticity in high-temperature Ni–Mn–Ga alloys. *J. Appl. Phys.* **2003**, *93*, 2394–2399. [[CrossRef](#)]
11. Chen, H.; Wang, Y.D.; Nie, Z.; Li, R.; Cong, D.; Liu, W.; Ye, F.; Liu, Y.; Cao, P.; Tian, F.; et al. Unprecedented non-hysteretic superelasticity of [001]-oriented NiCoFeGa single crystals. *Nat. Mater.* **2020**, *19*, 712–718. [[CrossRef](#)]
12. Ge, Y.; Heczko, O.; Söderberg, O.; Lindroos, V.K. Various magnetic domain structures in a Ni–Mn–Ga martensite exhibiting magnetic shape memory effect. *J. Appl. Phys.* **2004**, *96*, 2159–2163. [[CrossRef](#)]
13. Zhang, J.X.; Chen, L.Q. Phase-field model for ferromagnetic shape-memory alloys. *Philos. Mag. Lett.* **2005**, *85*, 533–541. [[CrossRef](#)]
14. Chmielus, M.; Zhang, X.X.; Witherspoon, C.; Dunand, D.C.; Müllner, P. Giant magnetic-field-induced strains in polycrystalline Ni–Mn–Ga foams. *Nat. Mater.* **2009**, *8*, 863–866. [[CrossRef](#)] [[PubMed](#)]
15. Dunand, D.C.; Müllner, P. Size effects on magnetic actuation in Ni–Mn–Ga shape-memory alloys. *Adv. Mater.* **2011**, *23*, 216–232. [[CrossRef](#)]
16. Wang, Z.L.; Zheng, P.; Nie, Z.H.; Ren, Y.; Wang, Y.D.; Müllner, P.; Dunand, D.C. Superelasticity by reversible variants reorientation in a Ni–Mn–Ga microwire with bamboo grains. *Acta Mater.* **2015**, *99*, 373–381. [[CrossRef](#)]
17. Zhou, Z.; Wu, P.; Ma, G.; Yang, B.; Li, Z.; Zhou, T.; Wang, D.; Du, Y. Large reversible magnetic-field-induced strain in a trained Ni<sub>49.5</sub>Mn<sub>28</sub>Ga<sub>22.5</sub> polycrystalline alloy. *J. Alloy. Compd.* **2019**, *792*, 399–404. [[CrossRef](#)]
18. Hua, H.; Wang, J.; Jiang, C.; Xu, H. Large reversible magnetostrain of a Ni<sub>30</sub>Cu<sub>8</sub>Co<sub>12</sub>Mn<sub>37</sub>Ga<sub>13</sub> single crystal. *Scr. Mater.* **2016**, *124*, 142–145. [[CrossRef](#)]
19. Yu, S.Y.; Gu, A.J.; Kang, S.S.; Hu, S.J.; Li, Z.C.; Ye, S.T.; Li, H.H.; Sun, J.J.; Hao, R.R. Large reversible magnetostrain in polycrystalline Ni<sub>50</sub>Mn<sub>33</sub>In<sub>17–x</sub>Ga<sub>x</sub>. *J. Alloy. Compd.* **2016**, *681*, 1–5. [[CrossRef](#)]
20. Zhong, Y.; Zhu, T. Phase-field modeling of martensitic microstructure in NiTi shape memory alloys. *Acta Mater.* **2014**, *75*, 337–347. [[CrossRef](#)]
21. Hu, C.; Zhang, Z.; Yang, T.; Li, W.; Chen, L. Phase-field simulation of magnetic microstructure and domain switching in (Tb<sub>0.27</sub>Dy<sub>0.73</sub>)Fe<sub>2</sub> single crystal. *AIP Adv.* **2021**, *11*, 015207. [[CrossRef](#)]
22. Wu, P.P.; Ma, X.Q.; Zhang, J.X.; Chen, L.Q. Phase-field simulations of stress-strain behavior in ferromagnetic shape memory alloy Ni<sub>2</sub>MnGa. *J. Appl. Phys.* **2008**, *104*, 073906. [[CrossRef](#)]
23. Wu, P.P.; Ma, X.Q.; Zhang, J.X.; Chen, L.Q. Phase-field simulations of magnetic field-induced strain in Ni<sub>2</sub>MnGa ferromagnetic shape memory alloy. *Philos. Mag.* **2011**, *91*, 2102–2116. [[CrossRef](#)]
24. Peng, Q.; He, Y.J.; Moumni, Z. A phase-field model on the hysteretic magneto-mechanical behaviors of ferromagnetic shape memory alloy. *Acta Mater.* **2015**, *88*, 13–24. [[CrossRef](#)]
25. Ren, X.; Wang, Y.; Zhou, Y.; Zhang, Z.; Wang, D.; Fan, G.; Otsuka, K.; Suzuki, T.; Ji, Y.; Zhang, J.; et al. Strain glass in ferroelastic systems: Premartensitic tweed versus strain glass. *Philos. Mag.* **2010**, *90*, 141–157. [[CrossRef](#)]
26. Wang, D.; Wang, Y.; Zhang, Z.; Ren, X. Modeling abnormal strain states in ferroelastic systems: The role of point defects. *Phys. Rev. Lett.* **2010**, *105*, 205702. [[CrossRef](#)]
27. Zhang, J.X.; Chen, L.Q. Phase-field microelasticity theory and micromagnetic simulations of domain structures in giant magnetostrictive materials. *Acta Materialia* **2005**, *53*, 2845–2855. [[CrossRef](#)]
28. Chen, L.Q.; Shen, J. Applications of semi-implicit Fourier-spectral method to phase-field equations. *Comput. Phys. Commun.* **1998**, *108*, 147–158. [[CrossRef](#)]
29. Khachaturyan, A.G. *Theory of Structural Transformations in Solids*; John Wiley&Sons: New York, NY, USA, 1983.
30. Tickle, R.; James, R.D. Magnetic and magnetomechanical properties of Ni<sub>2</sub>MnGa. *J. Magn. Magn. Mater.* **1999**, *195*, 627. [[CrossRef](#)]
31. Paul, D.I.; Marquiss, J.; Quattrochi, D. Theory of magnetization: Twin boundary interaction in ferromagnetic shape memory alloys. *J. Appl. Phys.* **2003**, *93*, 4561. [[CrossRef](#)]
32. Glavatska, N.; Mogilniy, G.; Glavatsky, I.; Danilkin, S.; Hohlwein, D.; Beskrovnij, A.; Söderberg, O.; Lindroos, V.K. Temperature dependence of martensite structure and its effect on magnetic field induced strain in Ni<sub>2</sub>MnGa magnetic shape memory alloys. *J. Phys.* **2003**, *112*, 963. [[CrossRef](#)]
33. Dai, L.; Cullen, J.; Cui, J.; Wuttig, M. Elasticity study in ferromagnetic shape memory alloys. *MRS Proc.* **2004**, *785*. [[CrossRef](#)]
34. Bhattacharyya, S.; Heo, T.W.; Chang, K.; Chen, L.-Q. A phase-field model of stress effect on grain boundary migration. *Model. Simul. Mater. Sci. Eng.* **2011**, *19*, 035002. [[CrossRef](#)]